Version of Record: https://www.sciencedirect.com/science/article/pii/S1350448720302365
Manuscript_dc104783aa0a9f99b7166f38030d381c

Absorbed doses in bricks and TL-dosimeters due to anthropogenic and natural environmental radiation sources

Alexander Ulanowski[a,b], Mauritius Hiller[a,*], Clemens Woda[a]

[a]Helmholtz Zentrum München, Institute of Radiation Medicine,

Ingolstädter Landstraße 1, D–85764, Neuherberg, Germany

[b]International Atomic Energy Agency, A-1400 Vienna, Austria (current affiliation)

*corresponding author: mauritius.hiller@gmx.de

Abstract

Radiation doses accumulated in ceramic or brick and assessed by thermoluminescence (TL) or optically stimulated luminescence (OSL) measurements are commonly used as a source of independent dosimetric information, helpful for validation of retrospective estimates of population exposures to anthropogenic radiation sources. This work systematically evaluates contributions to the cumulative dose in brick samples located at different heights in a wall from anthropogenic and natural radiation sources and provides data for quantification of the natural background component of the total dose in the brick derived in TL/OSL-measurements. Al- and Cu-cased thermoluminescence dosimeters (TLD) based on Al_2O_3:C are used to measure contemporary doses in brick walls as benchmarks and for validation of the dose reconstruction procedures. Correspondingly, doses in TLD and in brick in the same locations and under the same irradiation conditions are obtained by Monte Carlo simulations of radiation transport in realistic geometries. The data obtained in the simulations indicate that energy response of Al-cased dosimeters agrees better with the energy response of the brick than the response of Cu-cased TLD. The derived dosimetric data and relationships between doses in TLD and in

© 2020 published by Elsevier. This manuscript is made available under the Elsevier user license
https://www.elsevier.com/open-access/userlicense/1.0/

brick are systematically derived for different locations in the wall and above the ground and are be used in other dose reconstruction studies with luminescence techniques.

Keywords

1. Thermoluminescence/Optically Stimulated Luminescence 2. TLD, Al_2O_3:C 3. Retrospective Dosimetry 4. Environmental Radiation

1 Introduction

Luminescence measurements of quartz grains contained in ceramic and building materials have been widely used to retrospectively estimate radiation dose accumulated in these materials due to various environmental radiation sources (Meckbach et al. 1996; Taranenko et al. 2003; Bailiff et al. 2004a, b; Göksu and Bailiff 2006; Göksu et al. 2006; Woda et al. 2009, 2011, 2020, Hiller et al. 2017). Samples of such materials being collected in places contaminated by radiation sources of anthropogenic origin can serve as 'detectors' and provide unique objective information on actual radiation doses accumulated by environmental objects in such places. This information can become helpful for validating dose estimates derived via modelling or instrumental dose reconstruction.

The population of villages along the Techa River in the Southern Urals, Russia was exposed to elevated levels of anthropogenic radiation since the late 1940s due to discharges of radioactive waste from a nuclear reprocessing plant, the Mayak Production Association (PA), into the Techa River. Following massive contamination of the upstream Techa River and its shores, the population of some settlements had been relocated, while in other non-evacuated settlements countermeasures had been taken in order to reduce use of contaminated water and to prevent people and livestock from accessing the contaminated shores. The population of these villages formed an epidemiological cohort, which is currently called Extended Techa River Cohort (ETRC), (Krestinina et al. 2013a, b; Schonfeld et al. 2013). Information on radiation exposure of the cohort members and their respective doses are contained in the so-called Techa River Dosimetry System (TRDS) see Degteva et al. (2000a, b; 2012).

As a part of the projects SOUL and SOLO funded by the European Commission, the external radiation exposures of residents of the villages of Metlino and Muslyumovo, located at the

shores of the Techa River at distances of approximately 7 km and 78 km, correspondingly, downstream from the release point at the Mayak PA, were reconstructed and validated via application of new independent measurements using luminescence techniques. While Metlino was evacuated in 1956, seven years after the contamination begun, Muslyumovo was still inhabited at the time of the above-mentioned projects. The anthropogenic radiation doses accumulated in bricks of the buildings located at the shores of the Techa River were used to validate the model estimates of the population doses made in the TRDS (Hiller et al. 2017).

During 2006–2008, a series of field investigations were performed in Muslyumovo resulting in collection of brick samples, extensive radiation transport modelling efforts and depositing thermoluminescence detectors (TLD) to measure contemporary (gamma) dose rates for validation of the transport calculations. A similar series of measurements was carried out in Metlino between 2011 and 2013. At the time of the field studies, the radioactive contamination in Metlino and Muslyumovo was mostly represented by the long-living radionuclides ^{137}Cs and ^{90}Sr (Degteva et al. 2006). Results of the validation and estimates of cumulative air kerma values have been published previously (Woda et al. 2011, 2020; Hiller et al. 2017).

The collected brick samples were used as a source of information on integral anthropogenic absorbed dose inside the brick walls during the whole period since the radioactive releases started. Translation of the measured absorbed doses in brick samples to integral air kerma above the contaminated floodplain, which values are of the main interest for reconstruction of doses for the population, was performed using sophisticated Monte Carlo simulations of radiation transport in the contaminated terrain and the brick buildings, where the samples were collected from. Plausibility of the transport simulations have been validated by comparing calculated and measured contemporary dose rates above the floodplain and inside the brick

walls at various locations. For this purpose, an intensive survey to map contamination on the site, dose rate measurements and placing TL-detectors in the boreholes after collection of the brick samples were used to benchmark the computational model and techniques used.

In the Muslyumovo investigations, Al_2O_3:C TLD chips in a Cu-casing were used, in the investigations in Metlino, measurements from the same TLD chips in Al- and Cu-casings were used and compared. Both, Al- and Cu-shielded TLDs were placed in the brick walls, retrieved after one year and the absorbed doses in the TLDs were measured. However, for the dose reconstruction, not doses absorbed in TLDs are of interest, but the doses absorbed at the location of the TLDs in the bricks themselves. Consequently, the question arises on how to convert TLD readings into absorbed doses in the solid brick at the sample and TLD locations. Developing of pertinent data to facilitate such conversion is the first of the two main goals of the present study.

The second main goal of the study is related to another issue of luminescence dosimetry with building materials in contaminated settlements; namely, that part of the total dose accumulated in brick or ceramic is created by natural sources of radiation. This part appears as a background to be extracted in order to estimate the anthropogenic dose. Relative contribution of background to the total dose varies at various sites from negligible on the highly contaminated site in Metlino to approximately 50% in Muslyumovo. Correspondingly, evaluation of the anthropogenic dose for sites with low anthropogenic contamination requires appropriate auxiliary data, currently incomplete or missing, for accurate and thorough evaluation of the background contribution to the total measured dose.

This paper deals with methodological aspects and provides necessary data for conversion of TL-detectors readings to corresponding absorbed doses in brick samples and to the appropriate evaluation of the background contribution to the total dose in brick.

2 Materials and Methods

2.1 TLDs

The studied object were the TL detectors applied in the field studies in the Techa River valley. Specifically, the TL-detectors used in the study were Al_2O_3:C chips of 1 mm thickness and 5 mm in diameter, which were placed in two different casing materials, 1 mm thick copper or 3 mm thick aluminium and then positioned in boreholes into the brick wall at a depth of approximately 1 cm. The casing shields the TLD against alpha- and beta-sources in brick wall. The cases containing the Al_2O_3:C chips were sealed with a plastic (polyolefin) tube, which mechanically protected the cases and allowed for their appropriate positioning inside the brick wall (Fig. 1). After being exposed for approximately one year, the detector assemblies were extracted and delivered to the laboratory to be measured in a Risø TL-DA-12 reader (DTU Nutech). The results of the measurements express the absorbed dose in the Al_2O_3 chip in terms of the absorbed dose created during the exposure of the chip to a ^{137}Cs calibration source.

2.2 Sources of radiation exposure of brick and a detector

Dose accumulated in solid brick or in a TL detector is formed due to radiation coming from various natural and anthropogenic sources. The natural sources are due to cosmic radiation, due to ^{40}K and due to radionuclides from radioactive series, mainly the ^{238}U and ^{232}Th series.

Due to low abundance, the contribution from members of the ^{235}U series was neglected. The natural sources are located inside the solid brick as well as outside the brick wall. The anthropogenic sources are located outside the brick wall, for the case studied here, in radioactively contaminated soils near the wall. The part of absorbed dose in brick that is due to anthropogenic sources in soil is of main interest here and the TLD reading is used to validate its estimation.

Due to shielding by the cases and the plastic tubes, the TLD are not sensitive to alpha- and beta-radiation from the surrounding bricks. The quartz grains extracted from bricks were etched before luminescence measurements; the etching removes the outer quartz layer exposed to alpha particles. The etching procedure and the attenuation of external beta-radiation within the quartz grain reduce the average dose created by beta-particles approximately by 10% relatively to the "infinite matrix" beta-dose (Aitken 1985).

Summing up all above, the total absorbed dose in brick D_B and the total absorbed dose in TLD D_{TLD} can be represented as follows:

$$D_B = \overbrace{D_{B_{\gamma 1}}}^{\text{signal}} + \overbrace{D_{B\gamma_2} + D_{B\gamma_3} + D_{B_\beta} + D_{B_\alpha} + D_{B_C}}^{\text{background}}, \tag{1}$$

$$D_{TLD} = \underbrace{D_{TLD_{\gamma 1}}}_{\text{signal}} + \underbrace{D_{TLD_{\gamma 2}} + D_{TLD_{\gamma 3}} + D_{TLD_C}}_{\text{background}}, \tag{2}$$

where the sub-indices denote dose components due to:

γ_1 – gamma-radiation of anthropogenic radionuclides (ARNs) in soil;

γ_2 – gamma-radiation of natural radionuclides (NRNs) in soil;

γ_3 – gamma-radiation of NRNs in brick;

β – beta-radiation of NRNs in brick;

α – alpha-radiation of NRNs in brick;

c – cosmic radiation.

In the above equations (1) and (2), the components $D_{B_{\gamma 1}}$ and $D_{TLD_{\gamma 1}}$ are of principal interest for the dose reconstruction, considered as "the signal", all other components are regarded as background that need to be carefully evaluated and subtracted from the measured total values.

2.2.1 Radiation properties of natural radionuclides

In this study, the following radionuclides of primordial origin have been considered for calculating background dose contributions in Eq (1) and (2): ^{40}K, members of ^{238}U-, ^{232}Th-series taken at secular equilibrium.

2.2.2 Alpha-radiation of natural radionuclides

Alpha-particles emitted during the radioactive decay of members of the ^{238}U- and ^{232}Th- series expose the quartz grains in the brick. In the process of the sample preparation, the etching removes the quartz layers of the grain that were irradiated by the alpha-radiation so that their contribution to the total dose of brick can be further assumed zero and neglected: $D_{B_\alpha} \approx 0$. The TLD is completely shielded to alpha-radiation by the plastic tube and the casing material, therefore no contribution from alpha-emitters is included in Eq (2).

2.2.3 Beta-radiation of natural radionuclides

Etching and self-absorption reduce the absorbed dose in quartz grains due to beta-radiation to 90% of the "infinite matrix" dose, $D_{B_\beta}^{\infty}$ (Aitken 1985):

$$D_{B_\beta} \approx 0.9 D_{B_\beta}^{\infty} \quad (3)$$

The TLD casing also completely shields against the beta-radiation coming from natural radionuclides in the brick, so that no contribution from beta-radiation is included in Eq (2).

2.2.4 Cosmic radiation

The contribution from cosmic radiation was assumed to be equal for both the TLD and the brick:

$$D_{TLD_C} = D_{B_C} = S \quad (4)$$

The annual absorbed dose from cosmic radiation for the latitude of Muslyumovo or Metlino can be estimated to be about 0.20–0.24 mGy a^{-1} (UNSCEAR 2008, Woda et al. 2011).

The different densities of the considered materials (brick, Cu, Al, Al_2O_3) affect absorbed doses created by cosmic radiation and result in possible differences between them. However, in this work the difference between the brick and TLD with regard to cosmic radiation and its secondary radiations was neglected due to the low significance of this source and high energy of particles associated to it.

2.2.5 Internal sources of gamma radiation

Contributions of gamma-radiation from natural radionuclide sources within the brick (source term γ_3 in Eq (1) and (2)) were estimated in terms of the "infinite matrix" dose, $D_{B_\gamma}^{\infty}$, which is a dose created by gamma-emitters homogeneously distributed in an infinite brick wall. The 'infinite matrix' dose was calculated based on radiation emission data from the electronic version of the ICRP Publication 38 (ICRP 1983; Eckerman et al. 1994).

Absorbed doses in brick layers located closely to the "air-brick" interface are less than $D_{B_\gamma}^{\infty}$ because photons escaping from the wall into the air are unlikely to return. The absorbed dose

reduction due to vicinity of the interface can be accounted for, given the depth of the brick layer of interest is known. This reduction was estimated by Monte Carlo simulations, separately for photon emission spectra of the ^{40}K and of the equilibrium mixture of radionuclides from ^{238}U- or ^{232}Th- series, applying a simple geometry with a semi-infinite brick wall and the detection points inside the wall at various distances from the interface "air-brick".

2.3 Simulation of a realistic detector setup

The absorbed dose in the simulation of the coated TLD to photons emitted by the NRN in bricks is anticipated to differ from the brick absorbed dose because of the following reasons:

a) the detector itself and the shielding are purified materials and their contamination by NRN can be ignored;

b) the copper and plastic coatings of the detector provide shielding against radiation coming from outside;

c) during its exposition time, the detector is placed inside a drilled hole in the brick wall, which removes some brick medium and reduces the amount of source material adjacent to the detector.

The absorbed doses in the TLD were estimated by Monte Carlo simulations using the MCNP code (X-5 Monte Carlo Team 2003). A realistic setup was used to model the detector, its casing and its position inside the brick wall. A schematic view of the computational model of a Cu-cased TLD is shown in Fig. 1, as an example. The schematic view of the Al-cased TLD would appear similarly except for the 1 mm thick Cu-casing being replaced with the 3 mm thick Al-casing.

The photon source was sampled from weighted emission spectra of NRN uniformly distributed within infinite solid brick at distances up to 85 cm, thus allowing an appropriate accounting for effects of photon build-up and attenuation inside the brick.

2.4 External (environmental) sources of background gamma-radiation

Both the brick and the TLD are exposed to photons originated by NRN distributed in the environment outside the wall. The effect of these exposures is known to depend on ground terrain, physical properties of soil, soil water content, amount of vegetation on soil, concentration of NRN in soil, and height of a brick sample above the ground.

The natural radionuclides were assumed to be homogeneously distributed in soil. The absorbed doses in bricks at different depths inside the wall and at various heights above the ground were assessed by Monte Carlo simulations using a model of a simplified geometry consisting of an infinitely high and thick brick wall and an infinite ground area in front of the wall with radiation sources uniformly distributed in depth and in the area. The scoring regions are points above the soil and inside the wall. This modelling setup with extended sources and a very small (point) detector region is hardly suited for an analogue simulation; therefore, non-analogue point detector tallies and the DXTRAN technique (Lux and Koblinger 1991; X-5 Monte Carlo team 2003) were applied to calculate the absorbed doses in the bricks. The DXTRAN technique is a variance reduction method that enables Monte Carlo calculations to deterministically place particle tracks on spheres surrounding geometric regions of interest (Hiller and Hendrix, 2018).

The photon source in soil was modelled as uniformly distributed up to a depth of 50 cm and within a radius of 1000 m from the detector's projection on the ground. The point detectors

were placed at heights 1, 2, 5, 10, and 20 m above the ground level and inside the wall at depths 1, 3, 6, and 10 cm from the wall surface. Source energies were taken to represent the three separate groups of gamma-emitters in soil: ^{40}K and the nuclides of the ^{238}U- and ^{232}Th-series. The energies and yields of photons were taken from (ICRP 1983; Eckerman et al. 1994). The soil composition and density were taken from Eckerman and Ryman (1993).

Point detector tallies need to be applied with care because they are inversely proportional to distance between the particle's collision site and the target point, i.e. the tally's convergence can be affected by fluctuations due to near interaction events and the total run time needs to be increased to allow for a reliable compensation of such fluctuations and better statistics.

2.5 Properties of simulated materials

Table 1 lists elemental compositions and density of the materials used in radiation transport calculations. Air and soil properties are taken as appear in the Federal Guidance report 12, Eckerman and Ryman (1993) and the brick composition is taken from Taranenko et al. (2003).

2.6 Estimation of dose ratios 'TLD-brick'

Gamma-irradiation of the brick and of the TLD inside the wall apparently results in different absorbed doses in these receptors, whose ratio depends on the source energy and geometry of the system 'source-receptor'. Doses accumulated in TLD need to be related to doses in brick, thus conversion coefficients are needed, which express dose ratios 'TLD-brick' for various radiation sources and sample locations.

Consider a monoenergetic source S in soil and the target region T in the brick wall (Fig. 2). The target region can be either a solid brick wall or a hole filled by the TLD in its case and other wrapping materials (Fig. 1). Then the ratio R of absorbed dose in the target region T for the TLD, D_{TLD}, and for the brick, D_B, at the same place for the given source S with energy E is

$$R(E|T \leftarrow S) = \frac{D_{TLD}(E|T \leftarrow S)}{D_B(E|T \leftarrow S)}. \quad (6)$$

Generally, the ratio (6) could be computed using the same problem geometry as used in the calculation of doses in the brick due to NRN gamma sources in soil $D_{B_{\gamma 2}}$ (see Section 2.4). However, the use of point detectors is impossible as the dose receptors (TLD and brick) have different structure, which essentially defines energy-dependent ratio of their doses. At the same time, a straightforward analogue Monte Carlo simulation of photon transport from extended distant sources towards small detector regions is computationally ineffective and requires either using of variance reduction techniques or modifying the problem definition. Therefore, for this task, an alternative two-step approach was selected for calculation of the energy-dependent dose ratios, similarly to techniques used by Eckerman and Ryman (1993) to solve photon transport problems for small receptors and large 'source-receptor' distances.

Due to multiple scattering in soil and air, a monoenergetic isotropic photon source with energy E in soil produces at the wall surface a photon fluence with continuous energy spectrum $0 < E' \leq E$. Assuming that the replacement of brick with TLD has no influence on the energy spectra of photons originated from an external gamma-source in soil and incident on the

wall surface, one can introduce the wall surface as a coupling surface in the problem and, correspondingly, the dose ratio (6) can be factorised and written as follows:

$$R(E|T \leftarrow S) = \int_{E'} \int_{\Omega'} R_{c,\Omega}(E', \Omega'|T \leftarrow C)\, \phi_{\Omega}(E, E', \Omega'|C \leftarrow S) dE' d\Omega', \qquad (7)$$

where $R_{c,\Omega}(E', \Omega'|T \leftarrow C)$ is the ratio of doses 'TLD-brick' for photon source of energy E' incident on the coupling surface C at angle Ω', and $\phi_{\Omega}(E, E', \Omega'|C \leftarrow S)$ is the relative double-differential photon fluence at the wall surface produced by the isotropic volume source S in soil with energy E (MeV^{-1} sr^{-1}). Angular distribution of photons incident on the coupling surface can be further assumed as isotropic. This assumption can be regarded as plausible, taking into account an axial symmetry of the detector, large distances between the source and the detector regions, and effects of photon multiple scattering in soil, air and brick. Correspondingly, ignoring anisotropy of photon fluence at the height of the detector and neglecting the effect of the wall, Eq (7) can be simplified using angle-integrated energy-dependent quantities:

$$R(E|T \leftarrow S) = \int_{E'} R_c(E'|T \leftarrow C) \phi(E, E'|C \leftarrow S) dE'. \qquad (8)$$

Energy-dependent relative doses (dose per air kerma) for the considered targets, TLDs and brick, are smooth functions of energy, without sharp peaks or alternations and, correspondingly, the dose ratios 'TLD-brick' $R(E|T \leftarrow S)$ are smooth functions of energy, as well. Thus, for practical reasons, the integration over the continuous fluence spectrum in Eq (8) can be replaced by summation over the fluence spectrum in a group representation:

$$R(E|T \leftarrow S) \cong \sum_i R_c(E_i|T \leftarrow C) \bar{\phi}(E, E_i|C \leftarrow S) \Delta E_i, \qquad (9)$$

where E_i is the center energy of the i^{th} group; $\bar{\phi}(E, E_i|C \leftarrow S)$ (MeV^{-1}) is the relative photon fluence at the coupling surface averaged within the i^{th} energy group ΔE_i; $R_c(E_i|T \leftarrow C)$ is dose ratio 'TLD-brick' interpolated and evaluated for the energy E_i. The spectra are represented in 30 energy groups spanning the energy range 0.01–10 MeV. Boundaries of the energy groups are equally spaced on a log-scale. The Monte Carlo calculations were performed with MCNP (X-5 Monte Carlo Team, 2003) code using the technique described in (Saito and Jacob, 1995). A set of relative photon fluence spectra was computed for source energies ranging from 0.03 to 3 MeV at several heights above ground: 1, 2, 5, 10, 20, 50, and 100 m.

Finally, for the given geometrical configuration of the source and target regions and for a radionuclide source with a discrete energy emission spectrum, the dose ratio 'TLD-brick' was evaluated as follows:

$$R(T \leftarrow S) = \sum_j \sum_i R_c(E_i|T \leftarrow C)\, Y_j \bar{\phi}\big(E_j, E_i\big|C \leftarrow S\big)\Delta E_i, \qquad (10)$$

where Y_j is the yield of photons with energy E_j per a nuclear transformation (decay) of the considered radionuclide source.

3 Results

This section provides all necessary data for assessment of the background dose in the solid brick and in the TLD as well as for conversion of absorbed dose in the TLD to absorbed dose in solid brick in the same location.

3.1 Doses in brick and TLD from internal gamma sources in brick

Contributions of gamma radiation coming from natural radionuclide sources within the brick were estimated in terms of the "infinite matrix". Resulting reduction factors were estimated with the help of Monte Carlo calculations using geometry of a semi-infinite brick matrix. The reduction factors are given as a function of the layer depth in the brick and compared to available literature data for sources in soil (Aitken 1985) in Table 2. Unlike the data from (Aitken 1985), the present data can be regarded as pertinent to conditions specific for TL measurements of brick samples.

The dose in brick massive and in a Cu-cased TLD in brick due to photons emitted by NRN in the brick were determined using Monte Carlo calculations. The calculated absorbed doses in the TLD chip and in the monolithic brick at depth 1 cm from the "air-brick" interface per unit concentration of NRN in the brick wall are given in Table 3 along with the dose coefficient for the infinite brick matrix. The fractions representing the absorbed dose in the TLD and in the brick at 1 cm depth in terms of the "infinite matrix" brick dose, $D_{B_\gamma}^{\infty}$, are also shown in Table 3.

3.2 Doses in brick and TLD from natural radionuclides in soil

The contribution of environmental sources in the soil in front of the brick wall to brick and Cu-cased TLD were assessed. For this, natural radionuclides of the ^{40}K, ^{238}U- and ^{232}Th-series at secular equilibrium uniformly distributed in soil were considered and absorbed doses at various heights above soil in open air and in the brick at different heights and depths from the "air-wall" interface were simulated. The dose coefficients were estimated using Monte Carlo simulation of radiation transport in soil, air and the brick wall by scoring in point detectors

located at heights 1–20 m above ground and inside the brick wall at depths in range 1–10 cm. The dose rates calculated using this method are given in Table 4.

3.3 Relationship between doses in brick and in TLD from external environmental gamma-sources

Absorbed doses in TLD placed in the brick wall differ from absorbed doses in the brick itself at the same location. Therefore, a translation of absorbed dose in TLD to absorbed dose in brick needs auxiliary data to appropriately convert various components of the total dose (see Eqs. 1 and 2).

In the first step, the energy dependence of TLD dose per air kerma ratio was investigated by simulating the dosimeter and its casing in two conditions: (a) exposed to a parallel monoenergetic photon beam (in air) and (b) exposed in the brick wall to an external isotropic, monoenergetic photon source. The simulations were performed for the TLD in the Cu-casing, for condition (b) also for the TLD in the Al-casing. The dose per air kerma ratio of the brick itself was also studied under condition (b), allowing to compare the dose per air kerma ratio of the TLD to that of the brick under the same exposure conditions. The calculated ratios of the absorbed dose per air kerma are shown in Fig. 3.

3.3.1 TLD energy response

When the Cu-cased TLD is inserted into a drill hole in the brick wall and exposed to a monoenergetic isotropic external photon source (grey triangles in Fig. 3), the absorbed doses in the TLD are approximately 20% less than in the open air (black circles in Fig. 3), for photon energies above 100 keV. For photon sources with energies less than 100 keV, the reduction of the Cu-cased TLD dose in brick relative to kerma in free air is even stronger.

For the case of the TLD placed in the Al-casing, simulations were only done for the TLD in the brick wall (grey diamonds in Fig. 3). Compared to the Cu-cased TLDs, there is a similar behaviour for energies above 300 keV, but for lower energies an increase in the absorbed dose in the TLD with regard to the air kerma value is observed, up to a factor of almost 1.5 at approximately 70 keV.

For the case of the brick wall irradiated by the isotropic photon source (black squares in Fig. 3), the dose per air kerma ratio agrees again at the higher energies to that of both types of TLDs, but the dose per air kerma ratio of the brick is considerably larger than that of the TLDs for the source energies less than 300 keV. This means that low-energy photons result in higher brick doses compared to doses in the shielded TLD, thus a ratio of absorbed dose in the TLD and in the brick depends on the energy spectrum of photons incident on the wall surface. The difference in doses for low-energy photons is expected to be smaller for the Al-cased TLD than for the Cu-cased TLD.

3.3.2 Photon spectra from gamma-sources in soil

To assess appropriate conversion ratios, realistic spectra of photons incident onto the coupling surface (wall surface) originating from monoenergetic photon sources distributed in soil were calculated. Due to processes of scattering and attenuation in soil and in air, primary monoenergetic photons result in continuous energy spectra of photons above the ground.

As an example, the photon spectra at the heights of 1 m and 20 m above the ground produced by a monoenergetic 0.662 MeV photon source uniformly distributed in soil are shown in Fig. 4. As seen from the figure, the monoenergetic source in soil results in a continuous energy distribution of secondary photons. A large fraction of the secondary photons has energies less than 300 keV, i.e. is falling in the range where the differences in the doses for the same pho-

ton fluence between the TLD and the brick are maximal and increasing heights results in "softening" of the spectrum.

3.3.3 Conversion "TLD-brick"

The calculations were performed for various source energies of particles in the soil in the range from 0.01–3 MeV and altitudes of the TLD over the ground between 1 m and 100 m. The resulting curves give the relationship between dose measured in the brick and a dose measured in the TLD, for the TLD in Cu-casing (Fig. 5) and for the TLD in Al-casing (Fig. 6).

Finally, using the calculated dependencies (Figs. 5 and 6) the dose ratios can be computed for specific radionuclide sources of interest. For the considered situations of aged radioactive contamination of the environment, the relevant sources were: ^{137}Cs as an anthropogenic source and ^{40}K and members of ^{238}U- and ^{232}Th-series as natural ones. The resulting conversion ratios for these sources and various sample locations are shown in Table 5 and Table 6. The difference between the conversion ratio for ^{137}Cs in Table 5 and for a monoenergetic source in soil with 662 keV in Fig. 5 is explained by the fact, that for ^{137}Cs not only the main emission at 662 keV is taken into account (85 photons per 100 disintegrations) but also lower-energy X-rays (in sum around 7 emissions per 100 disintegrations, with energies around 30 keV), that are completely absorbed by the Cu casing but deposit dose in the brick massive (compare Fig. 3).

3.4 An example calculation for a brick sample

In order to illustrate the application of the different tabulated values, Table 7 gives an example for calculating the background dose rate in a brick sample from the wall of the mill in

Muslyumovo (Woda et al. 2011). The specific activity of natural radionuclides in brick was measured with low-level gamma spectrometry and converted to concentrations (ppm for ^{238}U and ^{232}Th and % for ^{40}K) in order to first calculate the infinite matrix gamma (not shown) and 90% of the infinite matrix beta dose rate using the conversion coefficients in Adamiec and Aitken (1998). From the fractions of the infinite matrix dose rate listed in Table 2, the fractional gamma dose rate at 1 cm depth in brick can then be calculated. For the site in Muslyumovo, specific activities of natural radionuclides in soil were also available from in-situ gamma-spectrometric measurements at different positions in front of the wall (Woda et al. 2011). These can then be combined with the coefficients from Table 4 to calculate the soil component of the gamma-dose rate in brick at the given sample height. As discussed in Woda et al. (2009, 2020), if no such data is available, country specific average radionuclide content in soil, as listed, e.g., in UNSCEAR (2000), can be used instead. As Table 7 illustrates, the contribution of the soil to the gamma dose rate is small, therefore a large uncertainty in this value will not have a significant impact. Using the total background dose rate and the (firing) age of the brick sample, the latter obtained from either dating of well-shielded bricks or from historical records, the background dose (equation 1) can then be calculated and subtracted from the total measured dose to obtain the anthropogenic dose in brick.

In principle, Tables 3 and 5 can be used in a similar fashion to calculate the background dose rate in TLD and from equation 2 the anthropogenic dose rate in TLD. The latter can then be converted using either Table 5 or 6, depending on the casing, to obtain the anthropogenic dose rate in brick due to ^{137}Cs distributed in soil (see e.g. Woda et al. 2020). Usually the brick to be measured is sampled first and TLDs then inserted into adjacent (intact) bricks for storage. If the latter are not separately sampled upon TLD retrieval, then the average and standard devia-

tion of the natural radionuclide content in the sampled (measured) bricks of the wall can be used to calculate an average background dose rate in TLD.

4 Discussion

The estimation of the fraction of the infinite brick matrix γ-dose rate at various depth into the brick for the ^{40}K-, ^{238}U- and ^{232}Th-series is consistent with the work by Aitken (1985), which presents the fractions for soil. All series show a fraction of 0.5 at 0 cm depth and from 0.85 to 0.9 at 10 cm depth. It is noteworthy that at 1 cm into the brick, a depth that is often used for measuring the anthropogenic dose in brick, the factors for the fractional dose rate are 20–30% higher than the value of 0.5, a value which was used in some previous studies (Bailiff et al. 2004a; Jacob et al. 2003; Göksu et al. 2002) but which is only valid at the direct brick-air interface.

The calculations of the γ-dose rate due to natural radionuclides in the brick are in the order of 10^{-3} mGy a^{-1} Bq^{-1} kg. With specific activities for the natural nuclides measured in bricks from the Southern Urals region, this γ-dose rate is about a factor of 1.6 to 2 smaller than the β-dose rate from the same nuclides within the brick (Woda et al. 2011, Woda et al. 2009).

The relative energy response (dose per air kerma) of the Al-cased TLD to photon sources in the energy range of 0.01–3 MeV has a closer resemblance to the energy response of brick than the energy response of the Cu-cased TLD. This is due to the lower atomic number of aluminium and the corresponding lower attenuation of photons with energies below 100 keV, an energy region where material composition becomes relevant, due to the dominating photoelectric effect. Consequently, the conversion ratios for calculating brick doses from TLD doses

are smaller in the case of Al-cased TLDs than for Cu-cased TLDs, although for ^{137}Cs the difference in the conversion ratios is only around 30%.

Looking at the conversion ratios for detector locations at different altitudes above the ground, there is a distinct height dependence of the conversion ratio for the TLD in Cu-casing. In contrast, the Al-cased TLD shows only little dependence to the height above ground. The reason for this lies in the overall shift of the spectrum of the photon fluence towards lower energies with increasing height (Fig. 4). Although the change is small it occurs in an energy region (below 100 keV), where the relative response of the TLD in copper and brick differ the strongest (Fig. 3). This effect is much less pronounced for Al-cased TLDs, again due to the better matching of the energy response of Al-cased TLDs and bricks.

5 Conclusions

This work provides the data useful for assessing background absorbed dose in brick or ceramic samples used in luminescence measurements supporting anthropogenic dose reconstruction studies. The presented dose coefficients for various components are generic and, due to this, can be applied in other dosimetric studies, especially, when improving significance of a weak anthropogenic signal requires accurate assessment of the background dose from natural sources.

This work supports the selection of TLD casing material and provides data for conversion of TLD doses to brick doses for comparative studies, where measured dose values of both, luminescence measurements in bricks and TLDs are used. Examples for such studies are found in dose reconstruction work, where absorbed doses in bricks are compared to contemporary annual doses, estimated by TLDs inserted in building walls (see e.g. Woda et al. 2009, Woda et

al. 2011, Hiller et al. 2017, Woda et al. 2020). As it was stated above, Al-cased TLDs have the advantage of showing a relative energy response which closer matches the one of bricks. Cu-cased TLDs are smaller in size, thus they might be useful when space limitation is an issue or only small drill holes can be made. Alternatively, if both types of casing are used then two independent assessments of the brick dose rate can be obtained, which also gives information about the accuracy of the conversion ratios. These results are pertinent to the specific TLD setups and only valid when using Al_2O_3 as a dosimeter material.

The results presented in this paper were obtained by Monte Carlo modelling of photon transport in simplified generic setups, assuming some representative properties of soil, brick and air. Uncertainties shown for the modelled quantities are solely due to statistical errors of the Monte Carlo estimates. In real life, variations of source-detector geometry, the source distribution in soil, elemental composition and density of the materials, physical approximations made will inevitably affect the quantities of interest and bring additional uncertainties into their estimated values. Therefore, it should not be forgotten that the computed and tabulated values presented in the paper, despite of being shown with three significant digits, are subjected in real life scenarios to additional uncertainties ranging from fractions of percent to tens of percent (e.g., use of the alternative soil composition from Saito and Jacob, 1995 increases "TLD/brick" ratios in Table 5 by 2–5%). Intended use of the quantities given in the paper is to be input for dose reconstruction calculations using the results of luminescence measurements of bricks; therefore, the numerical values are presented to avoid a possible rounding error bias in such computations. Investigation and quantification of the additional uncertainties of the estimates of the coefficients and ratios presented in the paper would require thorough consid-

eration of alternative computation scenarios and an extensive computational work, thus going beyond the purpose of the present work and setting a possible target for future studies.

Acknowledgements

The research leading to these results received funding from the European Community's Seventh Framework Program (FP7/2007-2013) under grant agreement n°249675 and the framework of the EC Integrated Project FP6-516478 SOUL (Southern Urals Radiation Risk Research). The authors thank the staff at Urals Research Center for Radiation Medicine (Chelyabinsk, Russian Federation), at Southern Urals Biophysics Institute (Ozersk, Russian Federation), at Mayak PA (Ozersk, Russian Federation) and, especially, Marina Degteva, Nikolay Bougrov, Alexander Akleev, Sergey Romanov, Yuri Mokrov, Yevgeni Vasilenko (deceased) and their colleagues for support and help during the field trips to Muslyumovo and Metlino.

References

Adamiec G, Aitken MJ (1998) Dose-rate conversion factors: update. Anc TL 16:37–39

Aitken MJ (1985) Thermoluminescence Dating. Academic Press: London and New York.

Bailiff IK, Stepanenko VF, Göksu HY, Jungner H, Balmukhanov SB, Balmukhanov TS, Khamidova LG, Kisilev VI, Kolyado IB, Kolizshenkov TV, Shoikhet N, Tsyb AF (2004a) The Application of Retrospective Luminescence Dosimetry in Areas Affected by Fallout from the Semipalatinsk Nuclear Test Site: An Evaluation of Potential. Health Phys 87:625-664.

Bailiff IK, Stepanenko VF, Göksu HY, Bøtter-Jensen L, Brodski L, Chumak V, Correcher V, Delgado A, Golikov V, Jungner H, Khamidova LG, Kolizshenkov TV, Likhtarev I,

Meckbach R, Petrov SA, Sholom S (2004b) Comparison of Retrospective Luminescence Dosimetry with Computational Modelling in Two Highly Contaminated Settlements Downwind of the Chernobyl NPP. Health Phys 86:25-41.

Degteva MO, Vorobiova MI, Kozheurov VP, Tolstykh EI, Anspaugh LR, Napier BA (2000a) Dose Reconstruction System for the Exposed Population Living Along the Techa River. Health Phys 78(5):542-554.

Degteva MO, Kozheurov VP, Tolstykh EI, Vorobiova MI, Anspaugh LR, Napier BA, Kovtun AN (2000b) The Techa River Dosimetry System: Methods for the Reconstruction of Internal Dose. Health Phys 79(1):24-35.

Degteva MO, Vorobiova MI, Tolstykh EI, Shagina NB, Shishkina EA, Anspaugh LR, Napier BA, Bougrov NG, Shved VA, Tokareva EE (2006) Development of an Improved Dose Reconstuction System of the Techa River Population Affected by the Operation of the Mayak Population Association. Radiation Research 166:255-270.

Degteva MO, Shagina NB, Vorobiova MI, Anspaugh LR, Napier BA (2012) Reevaluation of Waterborne Releases of Radioactive Materials from the Mayak Production Association into the Techa River in 1949-1951. Health Phys 102(1):25-38.

Eckerman KF, Ryman JC (1993) External exposure to Radionuclides in Air, Water, and Soil. Federal Ruidance Report No. 12. EPA Publication EPA-402-R-93-081. U.S. Environmental Protection Agency: Washington, DC.

Eckerman KF, Westfall RJ, Ryman JC, Cristy M (1994) Availability of Nuclear Decay Data in Electronic Form, Including Beta Spectra not Previously Published. Health Phys 67:338-345.

Göksu, HY, Degteva, MO, Bougrov, NG, Meckbach, R, Haskell, EH, Bailiff, IK, Bøtter-Jensen, L, Jungner, H, Jacob, P (2002) First international intercomparison of luminescence techniques using samples from the Techa River valley. Health Phys 82: 94-101.

Göksu HY, Bailiff IK (2006) Luminescence Dosimetry Using Building Materials and Personal Objects. Radiat Prot Dosim 119:413-420.

Göksu HY, Stepanenko VF, Bailiff IK, Jungner H (2006) Intercomparison of Luminescence Measurements of Bricks from Dolon Village: Experimental Methodology and Results of European Study Group. J Radiat Res 47(Suppl.): A29-A37.

Hiller M, Hendrix, J (2018) Effective use of DXTRAN in MCNP. 20th Topical Meeting of the Radiation Protection & Shielding Division of the American Nuclear Society. Santa Fe, NM, USA.

Hiller M, Woda C, Bougrov NG, Degteva MO, Ivanov O, Ulanovsky A, Romanov S (2017) External Dose Reconstruction for the Former Village of Metlino (Techa River, Russia) Based on Environmental Surveys, Luminescence Measurements, and Radiation Transport Modelling. Radiat Environ Biophys 56:139-159.

Jacob, P., Göksu, H.Y., Taranenko, V., Meckbach, R., Bougrov, N.G., Degteva, M.O., Vorobiova, M.I. (2003) On an evaluation of external values in the Techa River Dosimetry System (TRDS) 2000. Radiat. Environ. Biophys. 42: 169-174.

Krestinina LY, Davis FG, Schonfeld S, Preston DL, Degteva MO, Epifanova S, Akleyev AV (2013a) Leukaemia Incidence in the Techa River Cohort: 1953-2007. Br J Cancer 109:2886-2893.

Krestinina LY, Epifanova S, Silkin S, Mikryukova L, Degteva MO, Shagina N, Akleyev A (2013b) Chronic Low-Dose Exposure in the Techa River Cohort: Risk of Mortality from Circulatory Diseases. Radiat Environ Biophys 52:47-57.

ICRP (1983) Radionuclide Transformations: Energy and Intensity of Emissions. ICRP Publication 38. Ann. of the ICRP 11-13, Parts 1-2: 1-1250.

Lux I, Koblinger L (1991) Monte Carlo Particle Transport Methods: Neutron and Photon Calculations. CRC Press: Boca Raton, FL.

Meckbach R, Bailiff IK, Göksu HY, Jacob P, Stoneham D (1996) Calculation and Measurement of Depth Dose Distribution in Bricks. Radiat Prot Dosim 66:183-186.

Schonfeld S, Krestinina L, Epifanova S, Degteva MO, Akleyev A, Preston D (2013) Solid Cancer Mortality in the Techa River Cohort (1950-2007). Rad Res 179:183-189.

Saito K, Jacob P (1995) Gamma Ray Fields in the Air Due to Sources in the Ground. Rad Prot Dosim 58:29-45.

Taranenko V, Meckbach R, Degteva MO, Bougrov NG, Göksu Y, Vorobiova MI, Jacob P (2003) Verification of External Exposure Assessment for the Upper Techa Riverside by Luminescence Measurements and Monte Carlo Photon Transport Modeling. Radiat Environ Biophys 42(1):17-26.

UNSCEAR (2008) Sources and Effects of Ionizing Radiation. United Nations Scientific Committee on the Effects of Atomic Radiation UNSCEAR. Report Volume I: Sources. Report to the General Assembly Scientific. Annex B: Exposures of the public and workers from various sources of radiation.

UNSCEAR (2000) Report Volume I: Sources and effects of ionizing radiation; Annex B: Exposures from natural radiation sources. http://www.unscear.org/unscear/en/publications/2000_1.html

Woda C, Jacob P, Ulanovsky A, Fiedler I, Mokrov Y, Rovny S (2009) Evaluation of External Exposures of the Population of Ozyorsk, Russia, with Luminescence Measurements of Bricks. Radiat Environ Biophys 48(4):405-417.

Woda C, Ulanovsky A, Bougrov NG, Fiedler I, Degteva MO, Jacob P (2011) Luminescence Dosimetry in a Contaminated Settlement of the Techa River Valley, Southern Urals, Russia. Radiat Meas 46(3):277-285.

Woda C, Hiller, M, Ulanowski, A, Bugrov, NG, Degteva MO, Ivanov O, Romanov S, Tschiersch T, Shinonaga T (2020) Luminescence dosimetry for evaluation of the external exposure in Metlino, upper Techa River valley, due to the shore of the Metlinsky Pond: a feasibility study. Journal of Environmental Radioactivity, 214–215, 106152.

X-5 Monte Carlo Team (2003) MCNP - A General Monte Carlo N-Particle Transport Code, Version 5. Los Alamos National Laboratory: Los Alamos, NM.

Figures

Fig. 1. Schematic view of a coated TLD positioned inside a drill hole in a brick wall and picture of TLD chip and Al- and Cu-casing (inset). The TLD is placed at distance (a) 1 cm from the front of the bore hole. Its diameter (d) is 5 mm and thickness (b) is 1 mm. Thickness of the Cu-casing (c) is 1 mm (thickness of Al-casing is 3 mm, not drawn). The assembly is enclosed in a 1 mm thick PVC tube.

Fig. 2. Schematic (not to scale) view of the problem geometry layout used in the two-step calculations of doses in a brick wall produced by environmental gamma sources in soil.

Fig. 3. Absorbed dose per air kerma for the TLD in air, in the brick wall and for the brick itself at a depth of 1 cm.

Fig. 4. Photon fluence at different heights above ground created by a monoenergetic photon source with energy $\boldsymbol{E_0 = 0.662}$ MeV uniformly distributed in the upper 20 cm of soil

Fig. 5. Ratio of absorbed doses in the Cu-cased TLD and in brick at 1 cm depth due to monoenergetic photon sources uniformly distributed in soil. Indicated by arrows are the energies corresponding to principal photons produced due to decay of ^{40}K (1.46 MeV) and ^{137}Cs (0.662 MeV).

Fig. 6. Ratio of absorbed doses in the Al-cased TLD and in brick at 1 cm depth due to monoenergetic photon sources uniformly distributed in soil. Indicated by arrows are the energies corresponding to principal photons produced due to decay of ^{40}K (1.46 MeV) and ^{137}Cs (0.662 MeV).

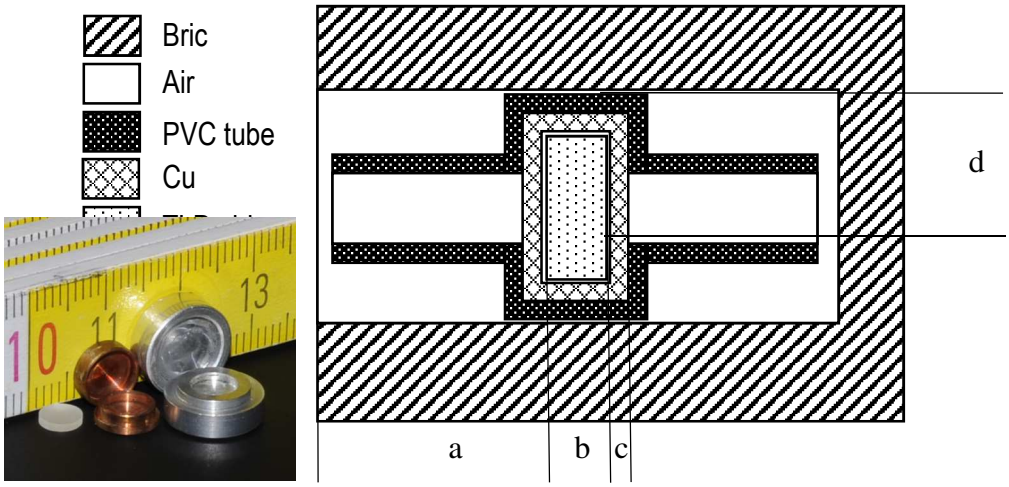

Fig. 1. Schematic view of a coated TLD positioned inside a drill hole in a brick wall and picture of TLD chip and Al- and Cu-casing (inset). The TLD is placed at distance (a) 1 cm from the front of the bore hole. Its diameter (d) is 5 mm and thickness (b) is 1 mm. Thickness of the Cu-casing (c) is 1 mm (thickness of Al-casing is 3 mm, not drawn). The assembly is enclosed in a 1 mm thick PVC tube.

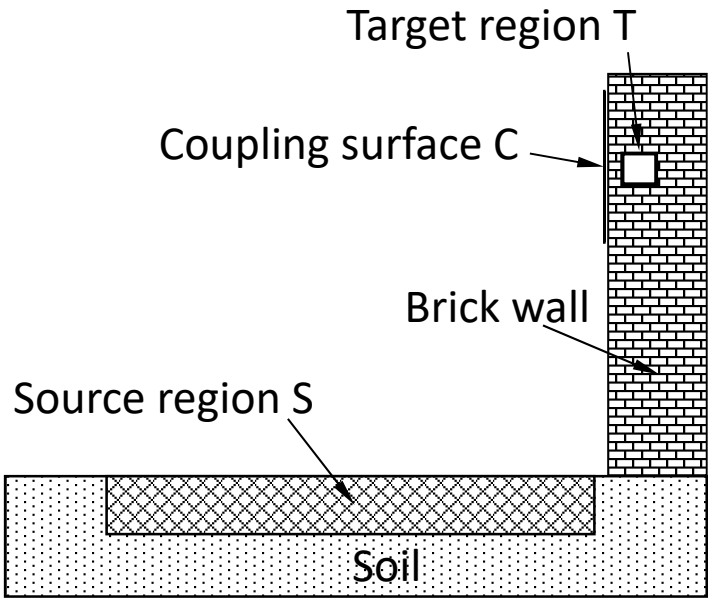

Fig. 2. Schematic (not to scale) view of the problem geometry layout used in the two-step calculations of doses in a brick wall produced by environmental gamma sources in soil.

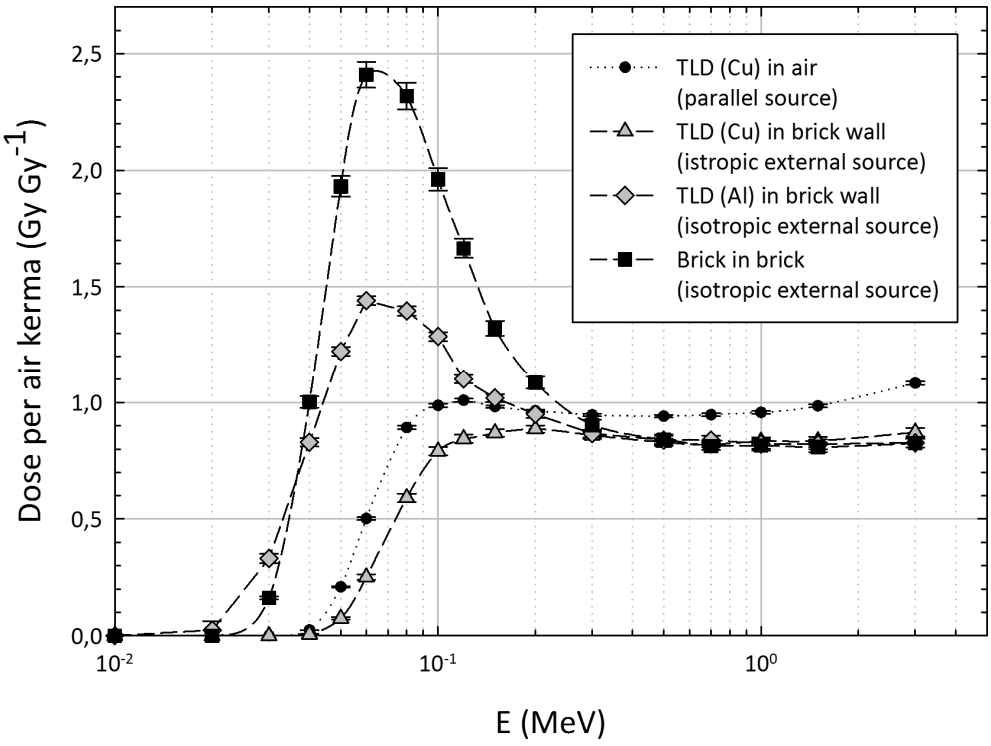

Fig. 3. Absorbed dose per air kerma for the TLD in air, in the brick wall and for the brick itself at a depth of 1 cm.

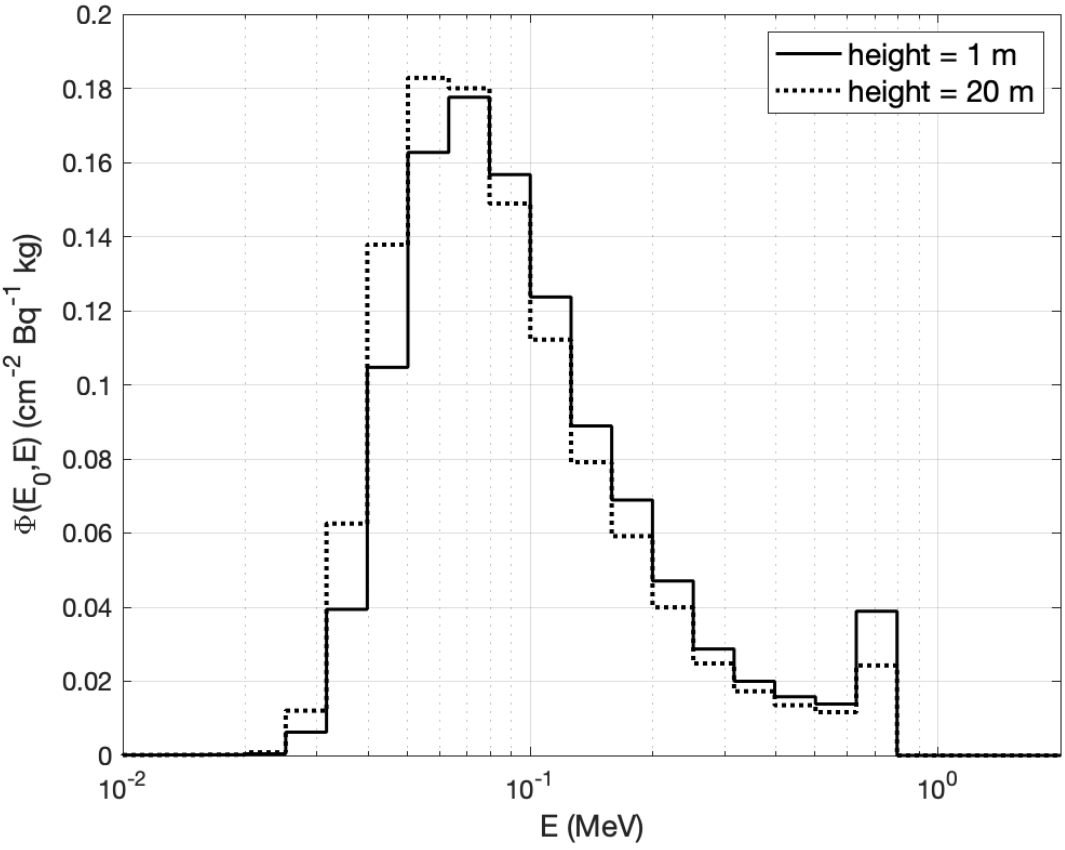

Fig. 4. Photon fluence at different heights above ground created by a monoenergetic photon source with energy $E_0 = 0.662$ MeV uniformly distributed in the upper 20 cm of soil

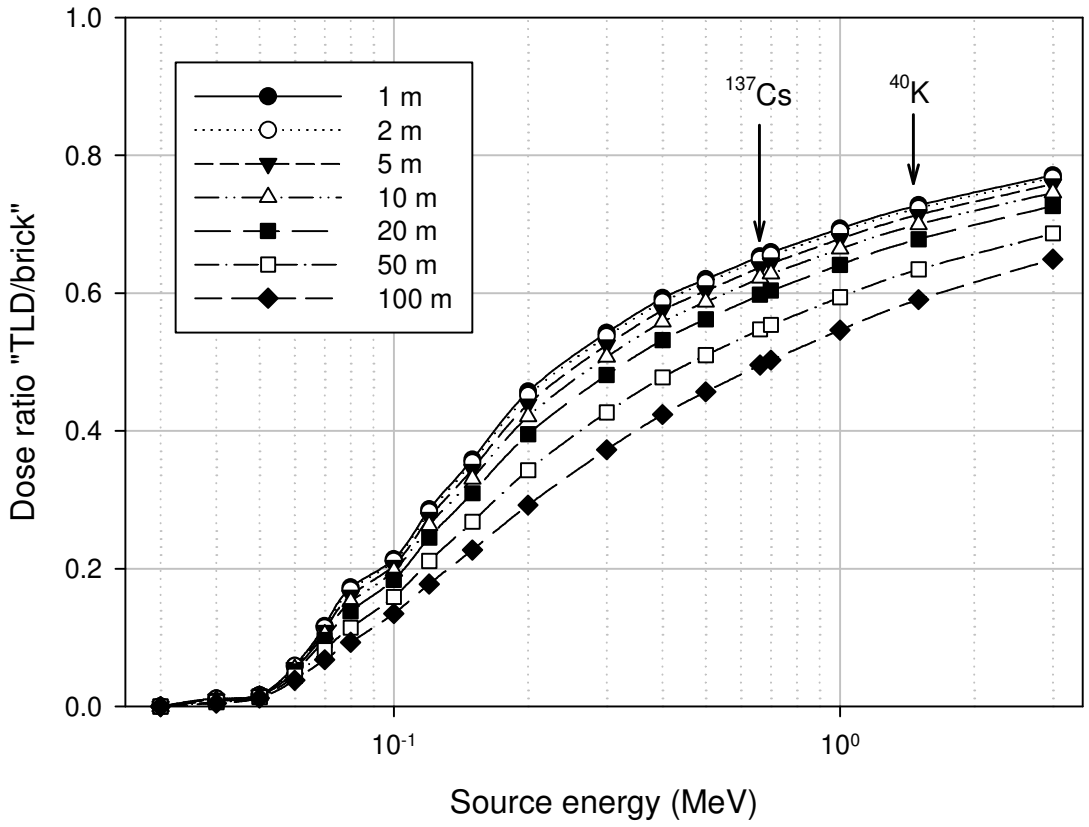

Fig. 5. Ratio of absorbed doses in the Cu-cased TLD and in brick at 1 cm depth due to monoenergetic photon sources uniformly distributed in soil. Indicated by arrows are the energies corresponding to principal photons produced due to decay of ^{40}K (1.46 MeV) and ^{137}Cs (0.662 MeV).

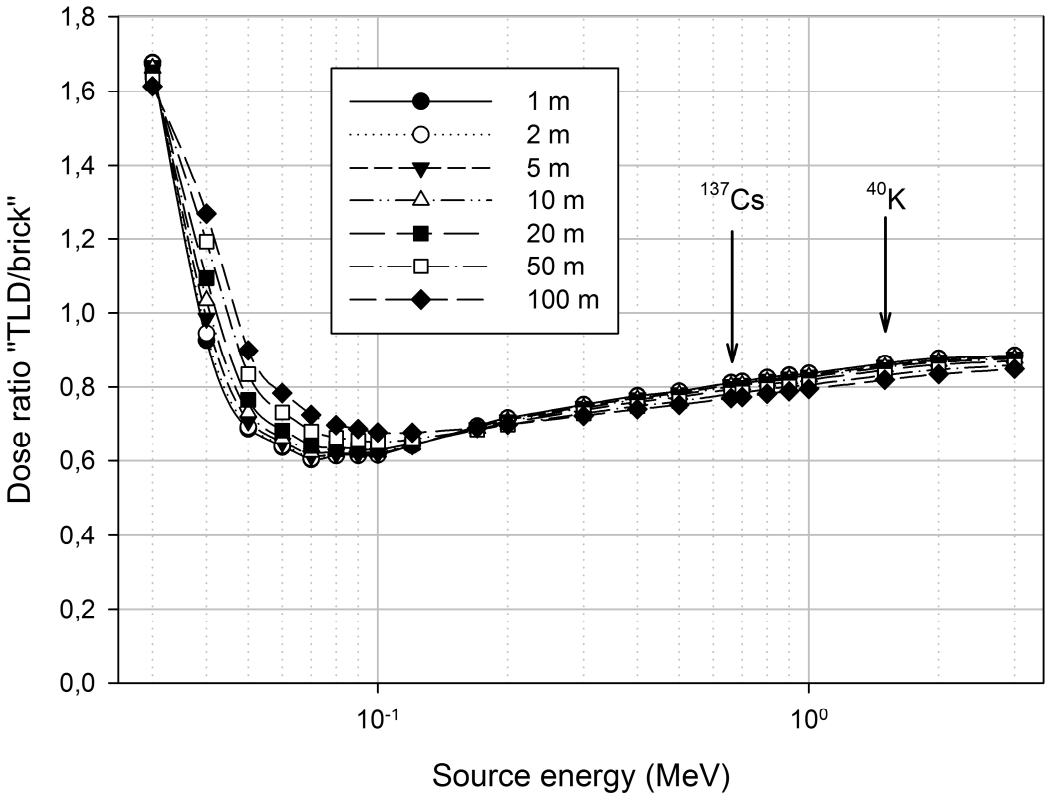

Fig. 6. Ratio of absorbed doses in the Al-cased TLD and in brick at 1 cm depth due to monoenergetic photon sources uniformly distributed in soil. Indicated by arrows are the energies corresponding to principal photons produced due to decay of ^{40}K (1.46 MeV) and ^{137}Cs (0.662 MeV).

Tables

Table 1. Elemental composition of the media used in the radiation transport calculation. Composition of air and soil are from the US Federal Guidance Report 12 (FGR12, Eckerman and Ryman (1993). Composition of brick (URCRM) is according to Taranenko et al. (2003).

Table 2. Fractions of "infinite matrix" dose at various depths from the interface "air-wall" for gamma radiation emitted by ^{40}K and radionuclides of the decay series of ^{238}U and ^{232}Th obtained in this work and similar fractions for soil medium from Aitken (1985).

Table 3. Absorbed dose rates in brick at 1 cm depth and in the TLD per unit activity concentrations of NRN in brick wall and as a fraction of "infinite matrix" dose.

Table 4. Absorbed dose rates due to natural radionuclides of ^{40}K, ^{238}U- and ^{232}Th-series in soil per unit activity concentration of the parent nuclide (mGy a^{-1} Bq^{-1} kg). Relative statistical errors in percent for P = 0.68 are shown in parenthesis.

Table 5. Ratio R of absorbed doses (see Eq. 6) in the Cu-cased TLD and bricks at 1 cm depth due to photons emitted by natural radionuclides and ^{137}Cs distributed in the environment.

Table 6. Ratio R of absorbed doses (see Eq. 6) in the Al-cased TLD and bricks at 1 cm depth due to photons emitted by natural radionuclides and ^{137Cs} distributed in the environment.

Table 7. Example calculation of background dose-rate at 1 cm depth in brick sample B3 from Muslyumovo (Woda et al. 2011). f (1 cm) is the fractional gamma dose rate at depth 1 cm, C the coefficient for converting activity in soil into dose-rate in brick at 1 cm depth for the sample height of 10 m. Uncertainties for P=0.68 are given for the sums of the dose rate contributions but are omitted for the sake of clarity for nuclide specific dose rate contributions.

Table 1. Elemental composition of the media used in the radiation transport calculation. Composition of air and soil are from the US Federal Guidance Report 12 (FGR12, Eckerman and Ryman (1993). Composition of brick (URCRM) is according to Taranenko et al. (2003).

Element	Z	Weight fraction for material:		
		Air (FGR12)	Soil (FGR12)	Brick (URCRM)
H	1	0.001	0.0021	
C	6	< 0.001	0.016	
N	7	0.751		
O	8	0.236	0.577	0.475
Na	11			0.005
Mg	12			0.017
Al	13		0.050	0.085
Si	14		0.271	0.296
S	16			0.002
Ar	18	0.013		
K	19		0.013	0.026
Ca	20		0.041	0.040
Ti	22			0.006
Fe	26		0.011	0.048
Density (g cm^{-3})		0.00125	1.6	1.8

Table 2. Fractions of "infinite matrix" dose at various depths from the interface "air-wall" for gamma radiation emitted by ^{40}K and radionuclides of the decay series of ^{238}U and ^{232}Th obtained in this work and similar fractions for soil medium from Aitken (1985).

Depth (cm)	Brick (this work)			Soil (Aitken 1985)[a]		
	^{40}K	^{238}U-series[b]	^{232}Th-series[b]	^{40}K	^{238}U-series[b]	^{232}Th-series[b]
0	0.5	0.5	0.5	0.5000	0.5000	0.5000
1	0.586	0.645	0.672	0.5938	0.6022	0.5974
3	0.682	0.747	0.763	0.7003	0.7156	0.7076
6	0.775	0.836	0.846	0.7964	0.8145	0.8055
10	0.852	0.903	0.909	0.8716	0.8879	0.8793
≥ 100	1.000	1.000	1.000	n.d.	n.d.	n.d.

[a] Precision of the displayed numbers follows that in Aitken (1985)
[b] Activities of parent nuclide and its progeny are taken in secular equilibrium

Table 3. Absorbed dose rates in brick at 1 cm depth and in the TLD per unit activity concentrations of NRN in brick wall and as a fraction of "infinite matrix" dose.

	Absorbed dose per unit concentration (mGy a^{-1} Bq^{-1} kg)			Fraction of "infinite matrix" dose $D_{B_\gamma}^{\infty}$		
	^{40}K	^{238}U-series	^{232}Th-series	^{40}K	^{238}U-series	^{232}Th-series
$D_{B_\gamma}^{\infty}$	7.89×10^{-4}	9.08×10^{-3}	1.28×10^{-2}	1.0	1.0	1.0
$D_{B\gamma_3}$	4.65×10^{-4}	5.24×10^{-3}	7.59×10^{-3}	0.586	0.645	0.672
$D_{TLD_{\gamma 3}}$	3.96×10^{-4}	3.63×10^{-3}	3.85×10^{-3}	0.503	0.400	0.383

Table 4. Absorbed dose rates due to natural radionuclides of ^{40}K, ^{238}U- and ^{232}Th-series in soil per unit activity concentration of the parent nuclide (mGy a^{-1} Bq^{-1} kg). Relative statistical errors in percent for P = 0.68 are shown in parenthesis.

Height (m)	In air	In brick at depth:			
		1 cm	3 cm	6 cm	10 cm
		^{40}K			
1	3.65×10^{-4} (0.1)	1.40×10^{-4} (3.6)	8.57×10^{-5} (4.0)	4.86×10^{-5} (4.4)	2.50×10^{-5} (4.7)
2	3.59×10^{-4} (0.1)	1.36×10^{-4} (2.9)	8.28×10^{-5} (2.4)	4.59×10^{-5} (2.5)	2.41×10^{-5} (2.8)
5	3.45×10^{-4} (0.1)	1.30×10^{-4} (1.1)	7.82×10^{-5} (1.3)	4.35×10^{-5} (1.6)	2.24×10^{-5} (2.4)
10	3.24×10^{-4} (0.1)	1.18×10^{-4} (0.8)	7.00×10^{-5} (0.8)	3.84×10^{-5} (0.8)	1.97×10^{-5} (1.0)
20	2.92×10^{-4} (0.1)	1.07×10^{-4} (1.9)	6.17×10^{-5} (1.0)	3.55×10^{-5} (5.5)	1.70×10^{-5} (2.5)
		^{238}U-series			
1	3.62×10^{-3} (0.1)	1.39×10^{-3} (4.8)	8.19×10^{-4} (6.6)	4.34×10^{-4} (5.4)	2.06×10^{-4} (6.2)
2	3.56×10^{-3} (0.1)	1.39×10^{-3} (2.9)	7.90×10^{-4} (3.2)	3.93×10^{-4} (2.6)	2.00×10^{-4} (3.0)
5	3.40×10^{-3} (0.1)	1.31×10^{-3} (2.6)	7.10×10^{-4} (1.3)	3.79×10^{-4} (1.7)	1.89×10^{-4} (2.6)
10	3.20×10^{-3} (0.1)	1.19×10^{-3} (1.1)	6.63×10^{-4} (1.1)	3.43×10^{-4} (1.5)	1.71×10^{-4} (2.1)
20	2.88×10^{-3} (0.1)	1.06×10^{-3} (1.3)	5.69×10^{-4} (0.9)	2.94×10^{-4} (1.8)	1.40×10^{-4} (0.8)
		^{232}Th-series			
1	4.80×10^{-3} (0.1)	2.08×10^{-3} (5.8)	1.24×10^{-3} (6.1)	7.01×10^{-4} (7.8)	3.50×10^{-4} (7.4)
2	4.72×10^{-3} (0.1)	1.89×10^{-3} (2.9)	1.13×10^{-3} (3.7)	6.17×10^{-4} (3.7)	3.38×10^{-4} (4.0)
5	4.53×10^{-3} (0.1)	1.75×10^{-3} (1.3)	1.04×10^{-3} (1.6)	5.93×10^{-4} (2.2)	3.09×10^{-4} (3.4)
10	4.27×10^{-3} (0.1)	1.62×10^{-3} (1.1)	9.47×10^{-4} (1.7)	5.34×10^{-4} (2.5)	2.71×10^{-4} (2.7)
20	3.85×10^{-3} (0.1)	1.41×10^{-3} (0.6)	8.15×10^{-4} (1.0)	4.44×10^{-4} (0.6)	2.35×10^{-4} (1.1)

Table 5. Ratio R of absorbed doses (see Eq. 6) in the Cu-cased TLD and bricks at 1 cm depth due to photons emitted by natural radionuclides and ^{137}Cs distributed in the environment

H (m)	Dose ratio 'Cu-TLD-brick' for nuclide:			
	^{137}Cs	^{40}K	^{232}Th-series	^{238}U-series
1	0.604	0.725	0.613	0.601
2	0.599	0.721	0.608	0.596
5	0.589	0.711	0.597	0.585
10	0.574	0.697	0.582	0.571
20	0.552	0.676	0.558	0.548
50	0.505	0.631	0.510	0.501
100	0.458	0.587	0.461	0.454

Table 6. Ratio R of absorbed doses (see Eq. 6) in the Al-cased TLD and bricks at 1 cm depth due to photons emitted by natural radionuclides and ^{137}Cs distributed in the environment

H (m)	Dose ratio 'Al-TLD-brick' for nuclide:			
	^{137}Cs	^{40}K	^{232}Th-series	^{238}U-series
1	0.812	0.703	0.582	0.572
2	0.810	0.698	0.577	0.567
5	0.806	0.688	0.566	0.557
10	0.801	0.675	0.551	0.543
20	0.794	0.653	0.528	0.521
50	0.781	0.609	0.482	0.476
100	0.770	0.566	0.436	0.433

Table 7. Example calculation of background dose-rate at 1 cm depth in brick sample B3 from Muslyumovo (Woda et al. 2011). f (1 cm) is the fractional gamma dose rate at depth 1 cm, C the coefficient for converting activity in soil into dose-rate in brick at 1 cm depth for the sample height of 10 m. Uncertainties for P=0.68 are given for the sums of the dose rate contributions but are omitted for the sake of clarity for nuclide specific dose rate contributions.

NRN	Brick: Concentration (ppm U/Th; % K)	f (1 cm)	$\dot{D}_{B\gamma_3}$ (mGy a^{-1})	$\dot{D}_{B\beta}$ (mGy a^{-1})	Soil: A (Bq/kg)	C (mGy a^{-1} Bq^{-1} kg)	$\dot{D}_{B\gamma_2}$ (mGy a^{-1})
^{238}U	1.90 ± 0.12	0.645	0.14	0.25	12 ±7	1.19E-03	0.014
^{232}Th	6.53 ± 0.27	0.672	0.21	0.16	10 ± 2	1.62E-3	0.016
^{40}K	1.48 ± 0.05	0.586	0.21	1.04	236 ± 24	1.18E-4	0.028
Sum			0.55±0.04	1.45±0.04			0.058±0.009

$\dot{D}_{B_{\gamma 2}} + \dot{D}_{B_{\gamma 3}} + \dot{D}_{B_\beta}$ (mGy a^{-1})	$\dot{D}_C$ (mGy a^{-1})	$\dot{D}_{\text{Background}}$ (mGy a^{-1})
2.06 ± 0.05	0.21 ± 0.05	2.28 ± 0.07